Journal of Catalysis **185,** 138–151 (1999)
Article ID jcat.1999.2465, available online at http://www.idealibrary.com on IDEAL®

Pd-*x*Mo/Al_2O_3 Catalysts for NO Reduction by CO

Martin Schmal,*[,1] M. A. S. Baldanza,* and M. Albert Vannice†

*NUCAT/PEQ/COPPE and EQ–Federal University of Rio de Janeiro, P.O. Box 68502, Rio de Janeiro 21945-970 Brazil; and †Department of Chemical Engineering, Pennsylvania State University, University Park, Pennsylvania 16802

Received December 3, 1998; accepted March 8, 1999

The adsorption and reactivity of CO and NO in the CO + NO reaction on Pd/Al_2O_3 and Pd–MoO_3/Al_2O_3 catalysts was studied using DRIFTS, and the chemical state of the catalysts was examined by TRP and UV-DRS while the active sites were probed by TPD and chemisorption of CO and NO. The Pd8Mo catalyst presented a monolayer of Mo on an alumina surface resulting from a polymerization process, identified by DRS measurements. With increasing Mo content MoO_3 crystals are formed. Mo was reduced to Mo^{+4} at lower temperatures in the presence of palladium particles, which favored the formation of bimetallic particles that produce a different kind of site for this reaction. TPD results indicated that the presence of the Mo monolayer favors the formation of N_2 compared to the Pd/Al_2O_3 catalysts. DRIFTS results indicated NO adsorption on Pd^{+2}, Pd^0, and $Mo^{+\delta}$ sites as well as formation of isocyanate on the Pd8Mo catalyst, while CO adsorption occurred on Mo during the reaction at different temperatures. Activity studies showed that the Pd8Mo catalyst is much more active and more selective to N_2 than the monometallic catalyst. A model for the reaction is suggested which shows that $Mo^{+\delta}$ is a promoter in the catalytic cycle for NO reduction by CO.

INTRODUCTION

Recently, NO reduction by CO, CH_4, or H_2 over supported Pd catalysts has been intensively studied, and much effort has been made to better understand the mechanistic aspect of these reactions, which occur in exhaust catalysts. Because of high prices and scarcity of rhodium, it is important to find an alternative catalytic component, with one possibility being a catalyst containing a noble metal promoted by a suitable metal oxide. Thus, Ghandi and coworkers (1) started in the 1980s by adding Mo oxide to Pd and observing decreasing NH_3 formation during NO reduction compared to Pt/Pd catalysts, and Halasz *et al*. (2, 3) also confirmed better selectivity to N_2. Furthermore, they noticed that these systems were thermally more resistant. This kind of catalyst is used in car converters in Brazil and more than 1.5 million such converters are manufactured in this country.

[1] To whom correspondence should be addressed.

Lange *et al*. (4) presented a different system comprised of Pt/TiO_2/SiO_2 for NO reduction by H_2 and CO, but in this case the titanium oxide concentration was extremely high, thus lowering the surface area of the metal, although a promoting effect was achieved which reduced the reactivity temperature. Recently, Valden *et al*. (5) presented an interesting paper using Pd/La_2O_3/Al_2O_3 catalysts in which the reactivity between NO and CO and their adsorption was studied by TPD and IR. The latter techniques indicated different behavior, since NO was adsorbed molecularly on the support and lanthanum oxide, while NO dissociation followed by the formation of N_2 and N_2O was seen on all Pd catalysts. A more fundamental discussion was presented by Szanyi and Goodman *et al*. (6) after they examined the CO + NO reaction by TPD and TPRS, found it to be structure sensitive on different planes of palladium, and attributed the structure sensitivity to the stabilization of molecularly adsorbed NO relative to N_{ad} on Pd crystal planes.

The present paper focuses on the adsorption and reactivity of CO and NO on Pd/Al_2O_3 and Pd8MoO_2/Al_2O_3 catalysts characterized by DRIFTS and kinetic measurements. The chemical state of the catalysts was examined by TPR and UV-DRS, while the active sites were probed by TPD and the chemisorption of CO and NO in an effort to determine the promoting effect of the molybdenum oxide and the state of the adsorbed surface species as well as the structure of the interaction between the oxide and the palladium.

EXPERIMENTAL

The catalysts were prepared by a wet impregnation method using a γ-Al_2O_3 support from Engelhard, which had a surface area of 189 m^2/g and pore volume of 0.54 cm^3/g. First, the alumina was impregnated with ammonium heptamolybdate dissolved in water to vary the Mo content from 2 to 20 wt%. Previous results (7) have shown that the best dispersion was obtained holding the pH at 5.0. For good homogenous dispersion, this impregnation (6 cm^3 soln/g) was done in a rotator evaporator for 1 h. Excess water was eliminated at 353 K under vacuum, then the sample was

0021-9517/99 $30.00

dried at 383 K and calcined for 2 h under flowing air. In sequence, palladium nitrite dissolved in water containing 10% nitric acid was incorporated sequentially by impregnating the Mo/Al_2O_3 samples with this solution (6 cm^3/g) and holding the Pd concentration at 1 wt%, then following the same procedure for drying and calcining. One Pd/Al_2O_3 catalyst was prepared similarly for comparison.

Standard characterization by BET measurements and CO and H_2 chemisorption were performed in an ASAP 2000 system (Micromeritics) after purging with N_2 and drying at 393 K at a vacuum better than 10^{-8} bar. The surface areas were determined from nitrogen physisorption isotherms at 198 K. The metallic surface sites were counted by irreversible CO and H_2 adsorption determined from isotherms at room temperature.

The TPR experiments were performed with equipment described elsewhere (8) by flowing a mixture of 1.5% H_2 in He (AGA 99.99%) at 30 cm^3/min and using a heating rate of 5 K/min from room temperature to 1223 K. The H_2 consumption was calculated from the spectrum, which allowed determination of the degree of reduction of Pd and Mo, as well as the interaction between them. TPD profiles of CO and NO desorption from Pd and Pd8Mo catalysts were obtained after exposing the sample to pulses of either 5% CO in helium or 1% NO in helium at 300 K until saturation prior to thermal desorption, then raising the temperature at 20 K/min to 823 K using a He flow rate of 50 cm^3/min. The mass spectrometer was calibrated against helium mixtures containing specified concentrations of CO, NO, or N_2O or pure CO_2, H_2, N_2, and Ar. The experimental determination of the fragmentation pattern of each product was obtained by its introduction into the mass spectrometer separately. The distribution of desorbed products was calculated from the TPD spectra of individual mass fragments as follows. From the most intense fragment for each product (such as $m/e = 44$ for CO_2) the corresponding amounts of its other fragments (in this example, $m/e = 28$) were determined taking into account the inensity ratios of the mass fragments. After subtracting the contributions from carbon dioxide, the remainder of the signal for $m/e = 28$ was assigned to carbon monoxide. The same procedure was applied to the desorption spectra of compounds containing nitrogen atoms. The distribution of desorbed products was based on the number of carbon or nitrogen atoms desorbed. These experiments were conducted in the same reaction system, which was coupled to a quadrupole mass spectrometer (Balzers Model PRISMA).

UV-DRS (diffuse reflection spectroscopy) measurements were conducted with a Varian Cary 5 (Varian) spectrometer with alumina or Mo/Al_2O_3 used as the reference for the spectra, thus allowing observation of the structure of the molybdenum phases and their interaction with Pd.

XRD measurements using a FIENES Model D5000 diffractometer with Cu$K\alpha$ radiation were obtained for the Mo/Al_2O_3 samples, after calcination only, to give additional information about the structure of Mo on the alumina support.

The DRIFT spectra were obtained with an upgraded Sirius 100 FTIR system (Mattson Instruments) using a DRIFTS cell (HVC-DRP, Harrick Scientific). The system is described elsewhere in detail (9). The bottom of the sample holder was filled with approximately 50 mg of Al_2O_3, and 30 mg of the catalyst sample was then placed on top for the DRIFTS studies. These measurements were performed following a procedure similar to that used in the kinetic measurements or the sample was prereduced by flowing a H_2/He mixture, as described for the TPR experiments. Spectra were then obtained following the three sequential treatments: (1) a mixture of 0.6% NO in He was flowed for 30 min before purging with Ar; (2) 1.3% CO in He was flowed then purged with Ar; and finally (3) a mixture of 0.6% NO + 1.3% CO in He was flowed then purged with Ar. During each of these treatments the temperature was varied. The spectra were obtained after running for 30 min. The same interferograms consisted of 1000 signal scans obtained using a post amplifier gain of 4, an iris setting of 50, and a resolution of 4 cm^{-1}, as described elsewhere (9). Each interferogram was Fourier transformed to its frequency component spectrum. The ratio of this spectrum to the reference spectrum gave the transmittance spectrum from which the absorbance spectrum was obtained. Comparative spectra were obtained after adsorption and reaction at programmed multistep temperatures. The alumina support was used as the reference for each temperature.

NO reduction by CO was performed in a microreactor system connected to a gas chromatograph utilizing a Carbosieve Carboxen 1000 column for product stream analysis. A typical sample size was 50 mg and the space velocity was 37,000 h^{-1}. The pretreatment was done *in situ* by first flowing He, then switching to a flowing 3% H_2/97% Ar mixture, ramping the temperature from room temperature to 773 K at a heating rate of 10 K/min, holding at this temperature for 1 h, then cooling in He to the reaction temperature. The reaction feed was a mixture of 0.6% NO in He and 1.3% CO in He with the balance He (99.999%) and which was governed by mass flow controllers (Tylan, Model 260). The total flow rate was 40 ml/min in all experiments, and after 30 min under stabilized reaction conditions a sample was taken for GC analysis. The products were analyzed on line using a gas chromatograph with an oven temperature program starting at 228 K, holding for 5 min, ramping the temperature at 20 K/min to 423 K, then holding for 5 min. This allowed separation of all gas products and water. The calculated areas from the peaks were used with thermal response factors to determine molar flow rates of all components and calculate conversions and selectivities. The reaction was studied by choosing different ascending and descending temperatures. Beside the temperature variation,

the NO partial pressure was varied at one temperature and low conversions. Finally, at the standard reaction conditions with NO and CO, O_2 was added and varied at two different concentrations in order to follow the effect of O_2 on the NO reduction reaction. Some experiments were repeated twice to ensure reproducibility. Also, two sequential sets of experiments were conducted in a one-week period and the initial reaction conditions were then re-established to determine the stability of the catalysts.

RESULTS AND DISCUSSION

Table 1 lists the Mo and Pd contents and the corresponding surface areas of the different catalysts. The irreversible H_2 and CO uptakes are also given. Results show that the BET surface areas decrease with increasing Mo content and that molybdenum can also chemisorb CO after reduction, which could affect the corresponding active surface area of the Pd8Mo catalysts.

The XRD patterns for the different Mo/Al_2O_3 samples are presented in Fig. 1. Compared to the Al_2O_3 sample, $2Mo/Al_2O_3$ exhibits a similar spectrum, while with higher contents such as 14% Mo and 20% Mo, additional peaks appear between 20 and 30° with different intensities, indicating the presence of bulk MoO_3 phases. However, it is not clear to what extent crystalline phases exist in the $8Mo/Al_2O_3$ sample. This information is better obtained from the UV-DRS spectra shown in Fig. 2. The absorption band around 285 nm^{-1} with a shoulder near 250 nm that is observed with the 2Mo sample is shifted toward higher wavenumbers as the Mo content increases. In addition, the 8Mo sample presented a band similar to that for 14Mo and 20Mo although the XRD spectra indicated different structures. Therefore, the UV-DRS results give better evidence for the increasing formation of Mo species. Using as a reference $Na_2MoO_4 \cdot 2H_2O$, in which Mo^{6+} is tetrahedrally coordinated, or MoO_3, which has Mo^{6+} in octahedral coordination, respective absorption bands at 250 and 290 nm or 290 and 330 nm are obtained; thus it seems that Mo^{6+} is present in both coordination forms, with the octahedral coordination prevailing as the Mo content increases. Fournier and co-workers (10, 11) observed that the shift in the absorption bands toward higher wavenumber with increasing Mo content indicates polymerization of Mo species and implies that the first absorption band at 290 nm, already found by Raman, should be associated with Mo^{6+} cations which are in octahedral coordination. The UV-DRS

TABLE 1

Mo and Pd Contents, Surface Area, and Irreversible Adsorption for $Pd–Mo/Al_2O_3$ Catalysts

Sample	Mo content (%)	Pd content (%)	H_2 chem. (μmol/g)	CO chem. (μmol/g)	Surface area (m^2/g)
Al_2O_3	—	—	—	—	189
2Mo	1.95	—	0.070	0.87	166
8Mo	7.50	—	0.133	13.3	149
14Mo	13.7	—	0.287	39.0	128
20Mo	19.9	—	0.399	45.7	113
Pd/Al_2O_3	—	0.97	3.00	4.74	163
Pd8Mo	7.49	0.90	1.23	14.2	142

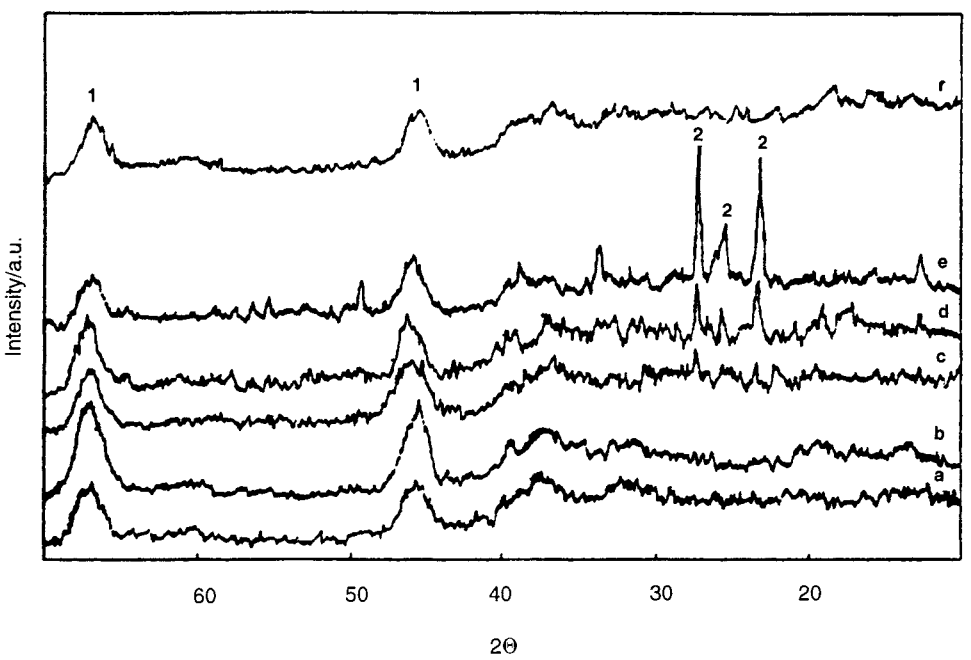

FIG. 1. X-Ray diffraction patterns: (a) Al_2O_3; (b) $2Mo/Al_2O_3$; (c) $8Mo/Al_2O_3$; (d) $14Mo/Al_2O_3$; (e) $20Mo/Al_2O_3$. (1) Al_2O_3 (2) MoO_3.

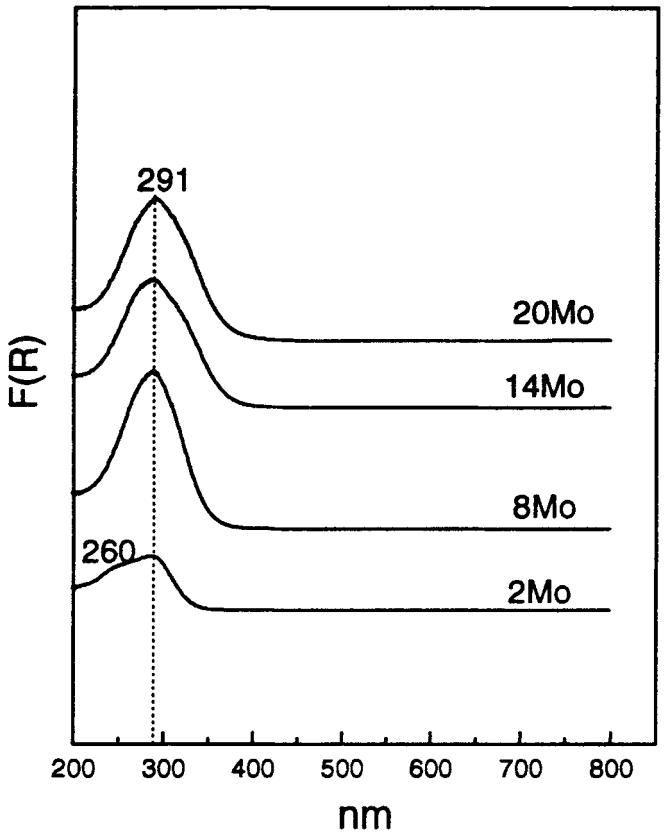

FIG. 2. Diffuse reflectance UV spectra of Mo/Al_2O_3 catalysts.

results with higher Mo-content catalysts exhibit absorption bands at 288 and 291 nm, which indicate three-dimensional structures of Mo oxide crystals. These results provide evidence that polymeric Mo species are responsible for the monolayer formation, while MoO_3 crystallites are formed at higher contents. The polymerization occurs according to the following reactions:

$$MoO_3 + H_2O \leftrightarrow MoO_2(OH)_2$$
$$MoO_2(OH)_2 + 2[OH]_{ads} \rightarrow \left[MoO_4^{2-}\right]_{ads} + 2H_2O$$
$$\left[MoO_4^{2-}\right]_{ads} \rightarrow \text{polymers.}$$

The UV-DRS results for the Pd8Mo catalyst presented in Fig. 3 display one peak at 288 nm and a shoulder around 436 nm when alumina is used as the reference (two bottom spectra). The PdO is partly masked by the presence of Mo, since Mo oxide exhibits a peak at 288 nm; however, when using the impregnated 8Mo sample as the reference for Pd8Mo (two upper spectra) to resolve only Pd bands, one can observe a peak at 416 nm, which corresponds to PdO crystals. Thus a broad peak around 334 nm, which is attributed to the presence of Pd–OH species on Pd/Al_2O_3 (upper spectrum) disappears indicating that a Mo overlayer was formed and that Pd was dispersed on this Mo species.

The TPR results for the different Mo/Al_2O_3 samples are displayed in Fig. 4. The profiles are very similar to others reported previously (12), and two different regions are typical for the H_2 uptakes. The first one around 750 K indicates the reduction of Mo^{6+} to Mo^{+4}, and the second one around 1212 K is related to Mo species which are difficult to reduce to Mo^0. The 14Mo and 20Mo/Al_2O_3 samples exhibit intermediate peaks around 850 K which are attributed to the reduction of bulk MoO_3 phases. These results are supported by the XRD and DRS data which confirm crystallites of the MoO_3 phase and the presence of Mo species in octahedral coordination.

Comparing the Pd8Mo sample (Fig. 5) with the corresponding 8Mo samples, it seems that palladium itself is easily reduced at room temperature and shows a desorption peak around 320 K which corresponds to β-Pd hydride decomposition. The presence of palladium modified the profile for Mo and shifted the reduction of Mo from 753 to 497 K, which indicates that Pd facilitates the reduction of Mo oxide and implies Pd may interact with these Mo species to possibly form a bimetallic compound; however, reduction of Mo oxide crystals still occurs at elevated temperatures around 1212 K, i.e., at the same temperature for Mo in the absence of Pd.

Figures 6 and 7 display the TPD profiles after CO adsorption on the Pd and Pd8Mo catalysts and show the

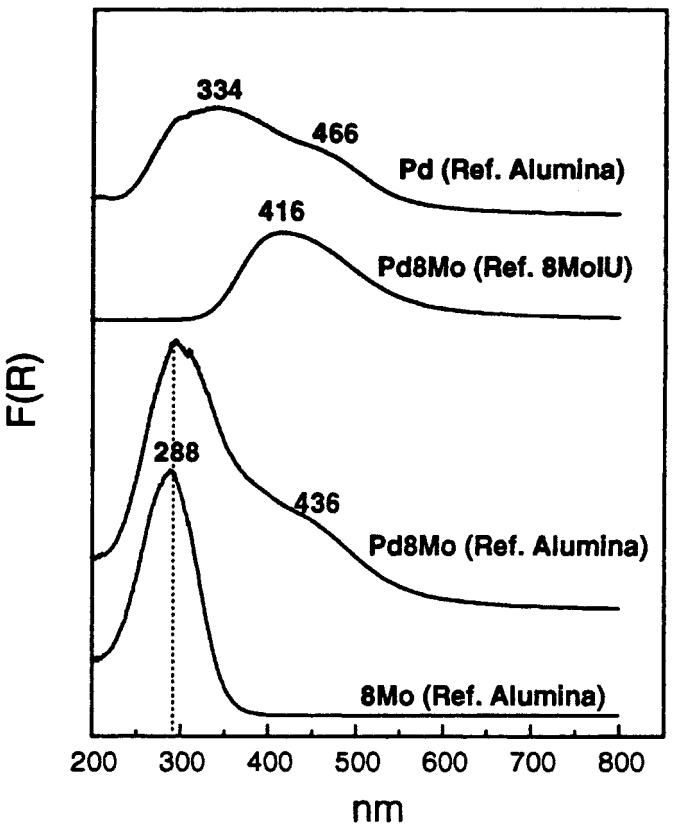

FIG. 3. Diffuse reflectance UV spectra of Pd8Mo/Al_2O_3 catalyst.

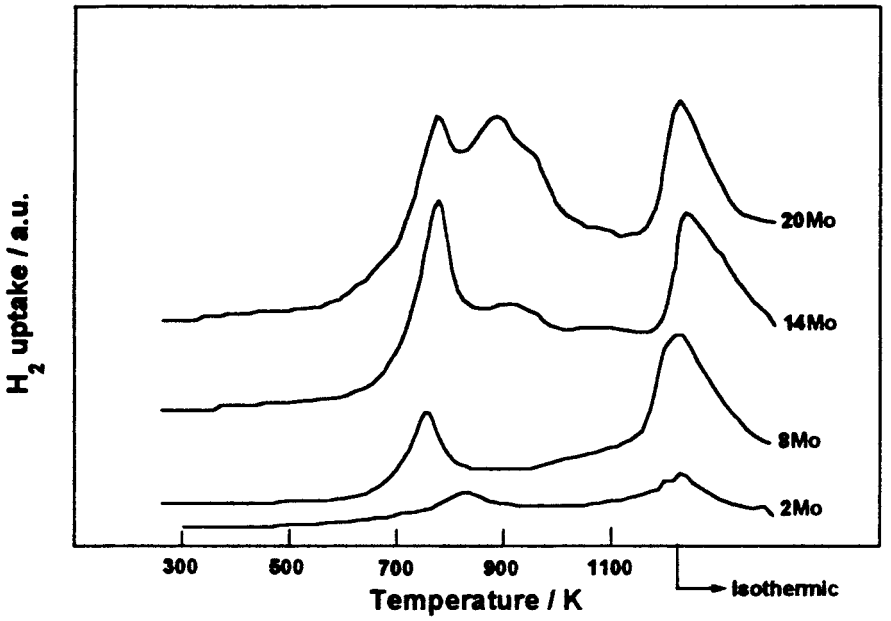

FIG. 4. Temperature programmed reduction profiles of Mo/Al_2O_3 catalysts.

corresponding formation of CO_2, H_2, and H_2O. These lineshapes exhibit two main peaks in distinct temperature ranges. A smaller peak near 400 K, present only with the Pd8Mo sample, corresponds to desorption of CO, while the maximum peak at 555 K follows CO_2 formation on both the Pd and Pd8Mo catalysts, which are very close to the profiles presented recently by Valden *et al.* (5). However, with Pd a second peak for CO appears around 823 K together with the formation of water, while with Pd8Mo only H_2 is seen at this temperature. The lineshapes with Pd8Mo are broad and different from those for the Pd catalyst. Contrary to the results of Valden *et al.*, the maximum desorption peak for CO is not shifted to lower temperature in the Pd8Mo catalysts, as observed for CO desorption from a $Pd/La_2O_3/Al_2O_3$ catalyst. On the other hand, CO_2 formation occurs soon after the small shoulder, which indicates no change in the CO bonding due to the Mo sites but, according to the literature, dissociation of CO should have occurred (13) with simultaneous formation of water beginning at 590 K, indicating side reactions with surface hydroxyls depending on the Mo loading. Moreover, H_2 formation was observed above 730 K with simultaneous CO desorption,

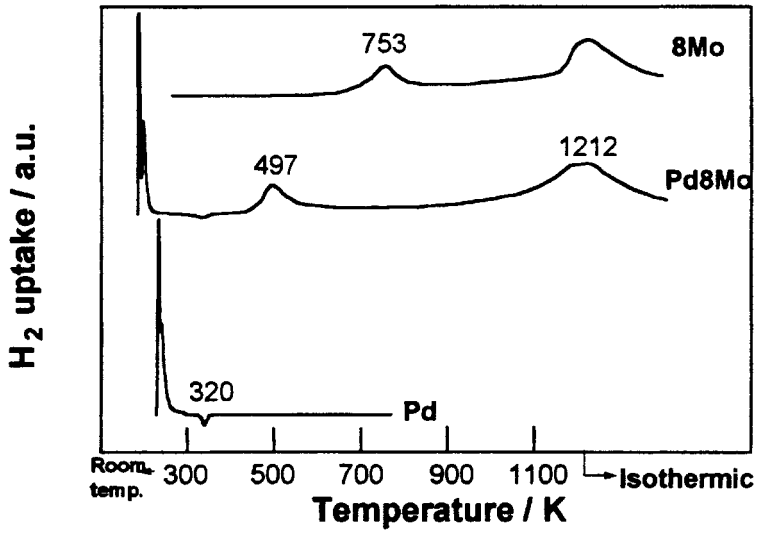

FIG. 5. Temperature programmed reduction profiles of 8Mo and Pd8Mo catalysts.

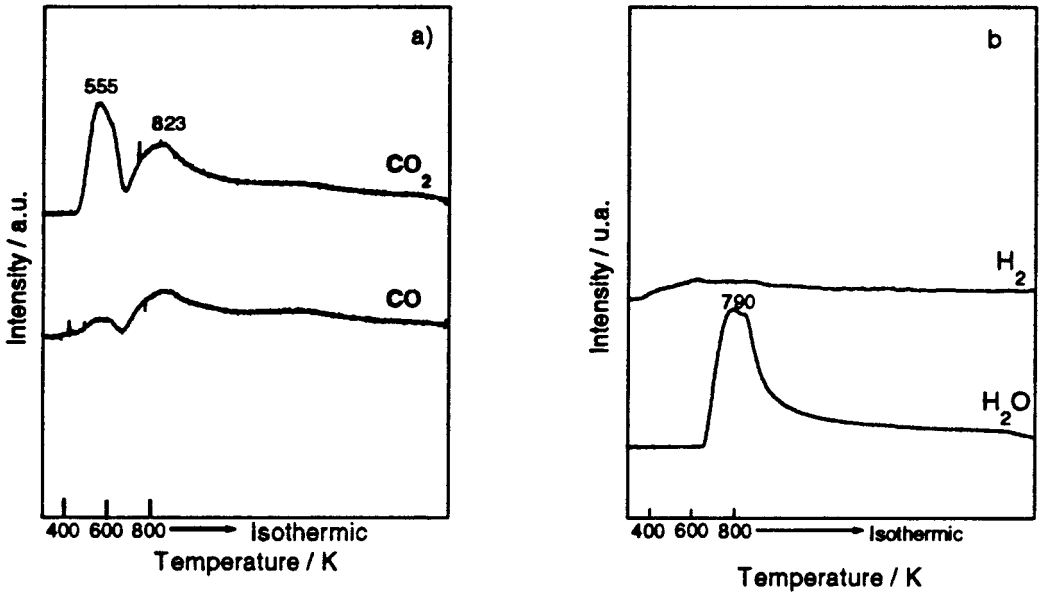

FIG. 6. TPD after CO adsorption on a Pd/Al_2O_3 catalyst.

which may be attributed to the presence of a Mo bronze at elevated temperature (14). This is confirmed by the TPD analysis of a 20% Mo/Al_2O_3 catalyst shown in Fig. 8.

The profile of Pd2Mo is completely changed as Mo concentration increases, which means that CO desorption prevails with a maximum at 410 K with little formation of CO_2. These results are in good agreement with Stara and Matolin for the adsorption/dissociation of CO on a Pd/Al_2O_3 catalyst (15). They found that CO dissociation was important on Pd particles smaller than 2.5 nm, with disproportionation also occurring and depending on the particle size. The smaller the crystallite size, the higher the carbon formation rate. From this point of view, it seems that the Pd particle size in the Pd and Pd8Mo catalysts covers a wide range, as observed from chemisorption data. In addition, it seems that the dissociation of CO may also be promoted by crystallographic effects of Pd in the presence of Mo oxide crystals, even with smaller Pd particle sizes.

Figures 9 and 10 display NO desorption profiles along with the corresponding formation of N_2 and N_2O for the

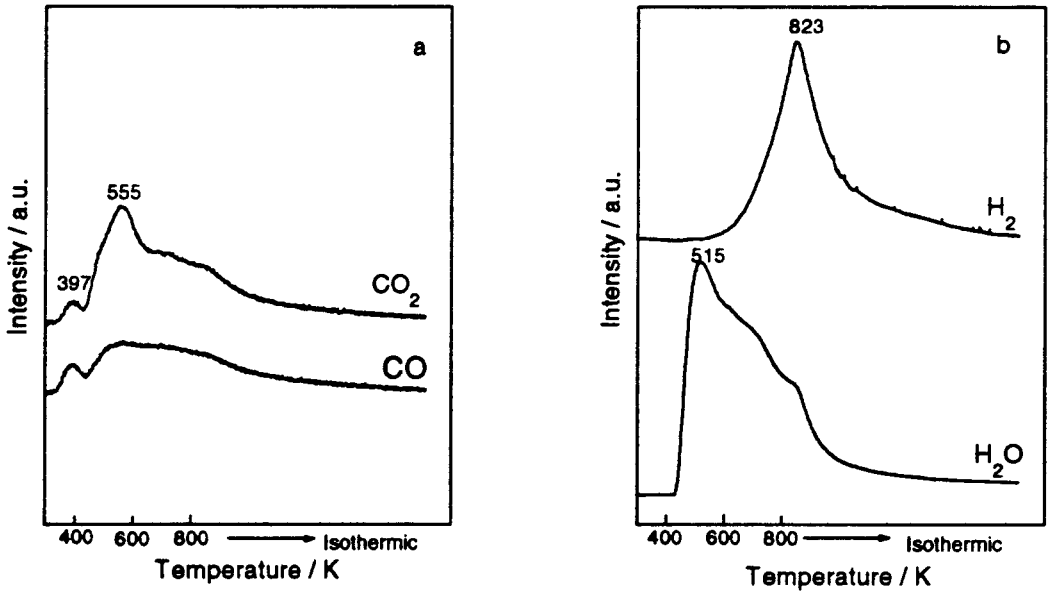

FIG. 7. TPD after CO adsorption on a Pd8Mo catalyst.

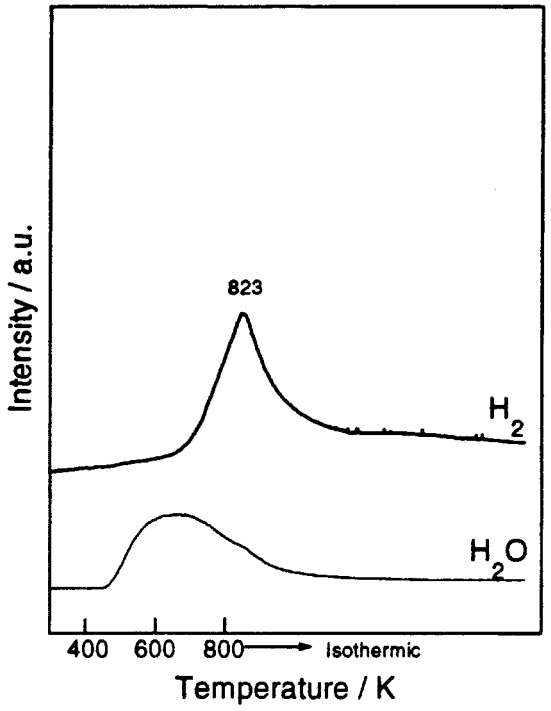

FIG. 8. Blank TPD with $20Mo/Al_2O_3$.

Pd and Pd8Mo catalysts. The lineshapes are quite different from the CO profiles and they vary between the two catalysts, indicating a different interaction of NO in the presence of Mo. On Pd NO desorption occurs with a peak maximum around 530 K with a weak peak at 350 K, while on Pd8Mo it desorbs more easily. However, the formation of N_2 and N_2O are markedly different. On Pd broad peaks exist around 780 K and above 800 K for N_2 and N_2O with no NO desorption, but these lineshapes are sharply modified in the presence of Mo, appearing as two well-defined peaks for N_2 at 542 and 772 K, yet no NO desorption is detected above 600 K. It clearly suggests side reactions which occur mainly on sites modified by Mo.

A fresh sample of Al_2O_3 was loaded in the DRIFTS cell and purged overnight in 40 ml/min of Ar at room temperature before exposing it to NO. A spectrum showed a band for OH groups around 3700 to 3630 cm^{-1} which was diminished by treatment at 473 K up to 623 K at temperature intervals of 20 K. An OH group linked to AlOOH was observed at 1049 cm^{-1} together with the 3764 cm^{-1} band. Residual carbonates were also observed but disappeared with increasing temperature (Fig. 11a).

The 20% Mo/Al_2O_3 sample was investigated similarly, first in the oxide form and then after reduction in a H_2/He mixture by raising the temperature to 773 K. Figure 11b displays the spectrum obtained after flowing NO at 573 K. The OH groups at 3705 and 3630 cm^{-1} were noticeably reduced together with the OH groups at 1385 cm^{-1}. Al_2O_3 exhibits bands from N_2O and NO gas molecules at 2242 to 2208 cm^{-1} and at 1916 to 1840 cm^{-1}, respectively, together with well-defined peaks at 1596 and 1385 cm^{-1} (Fig. 11a) with the latter two corresponding to nitrate or nitrous complexes and hydroxyls groups, respectively. This behavior is completely changed on Mo/Al_2O_3, which displays two other significant peaks at 1813 and 1724 cm^{-1} while the 1596 and 1385 cm^{-1} bands disappear. These two bands remain stable not only after purging with Ar, but also after submitting the same sample to reduction using flowing H_2 and NO at 573 K (Fig. 11c–11d).

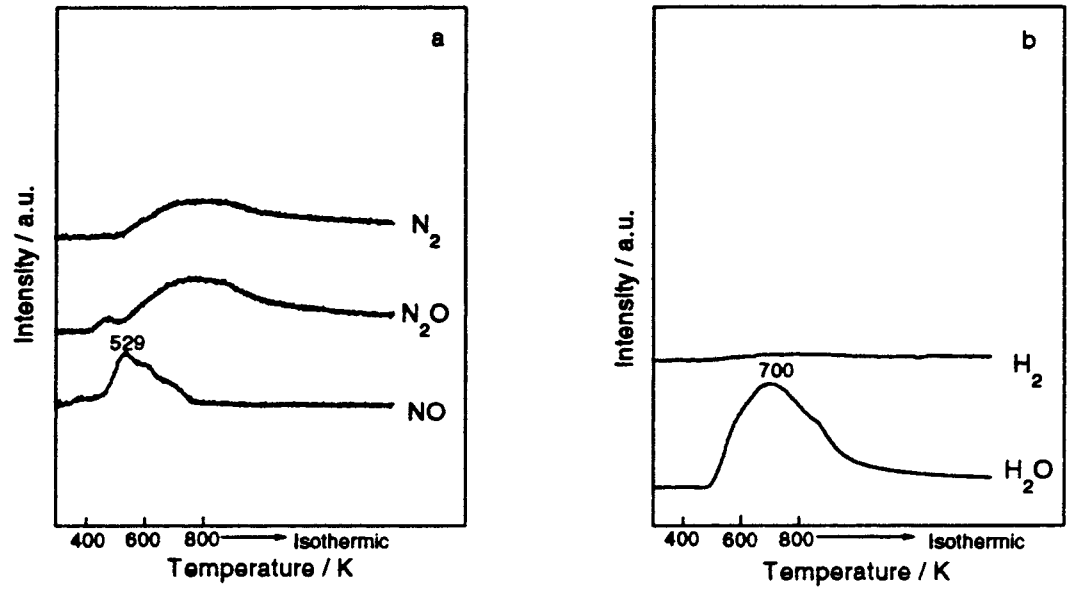

FIG. 9. TPD after NO adsorption on a Pd/Al_2O_3 catalyst.

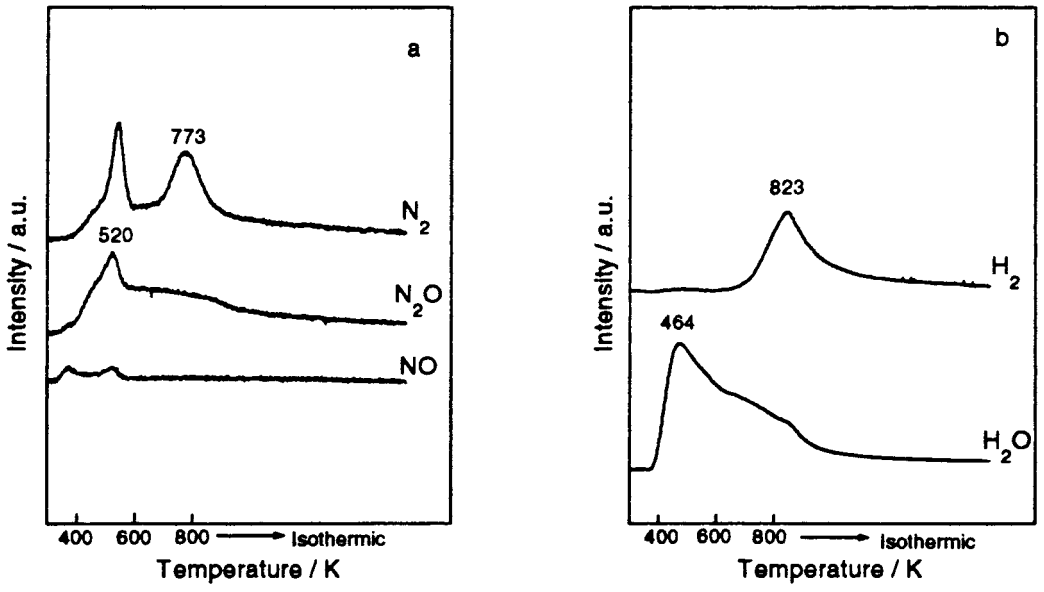

FIG. 10. TPD after NO adsorption on a Pd8Mo catalyst.

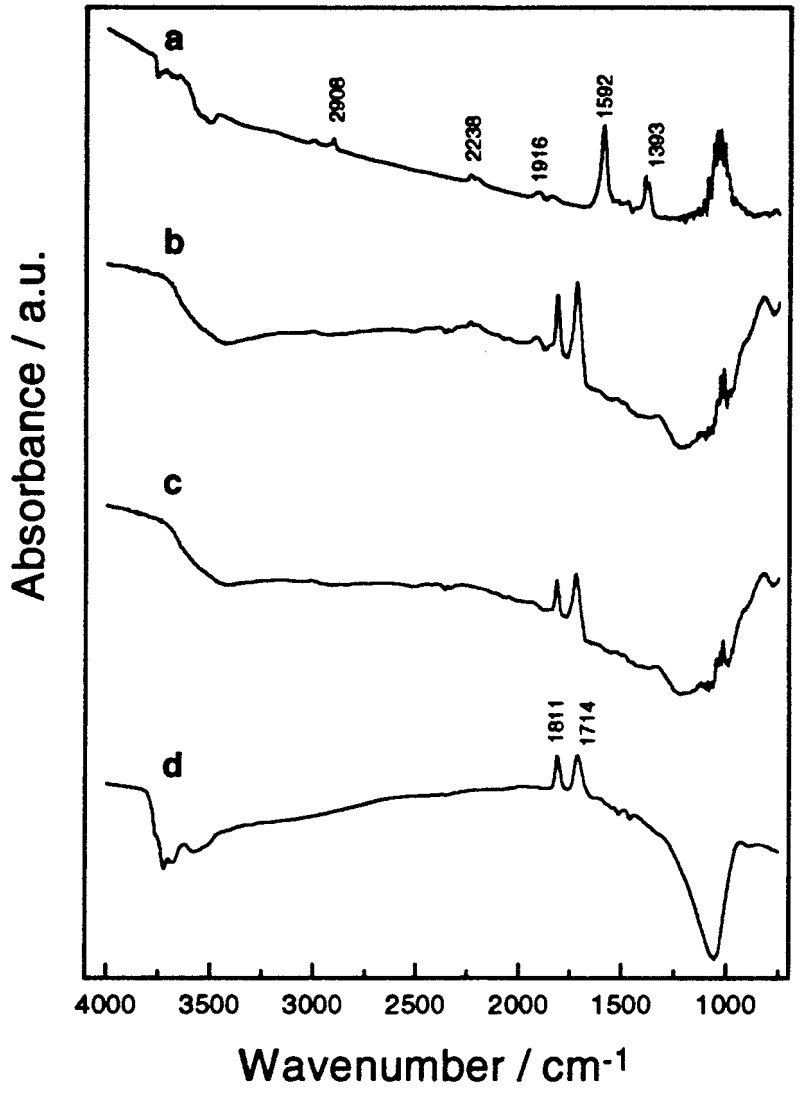

FIG. 11. DRIFT spectra at 573 K of (a) NO on Al_2O_3, (b) NO on Mo/Al_2O_3, (c) after purging with Ar, and (d) reduction of Mo/Al_2O_3 using $H_2 + NO$.

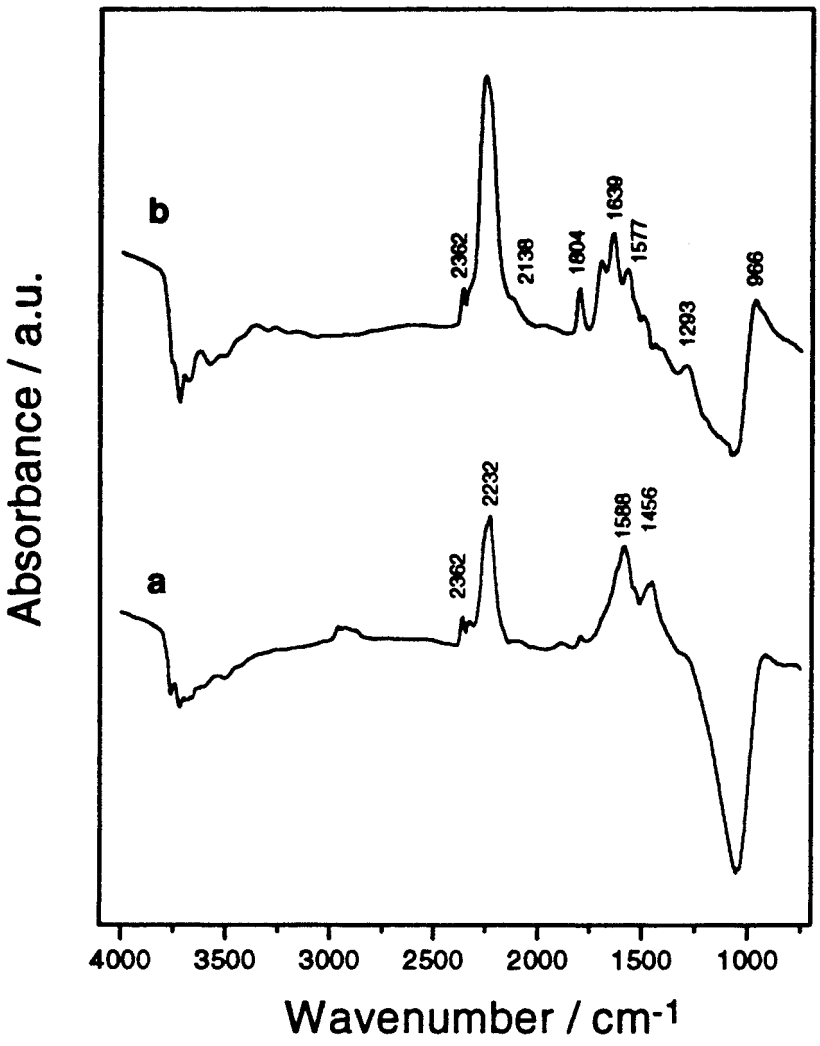

FIG. 12. DRIFT spectra at 573 K during the NO + CO reaction on: (a) Pd/Al_2O_3 and (b) Pd8Mo.

Figure 12b displays the peaks resulting from the NO + CO reaction on the Pd8Mo catalyst at 573 K in the DRIFTS cell, which can be compared to those from the Pd/Al_2O_3 catalyst (Fig. 12a). Beside the bands found on Pd/Al_2O_3, it exhibits new bands with quite different intensity. First, a small shoulder at 2138 cm^{-1} attributed to CO adsorption on Pd^{+2} can be seen. After purging with Ar, the CO_2 band is removed but the other bands remain. NO forms linear surface complexes on Pd between 1803 and 1577 cm^{-1}, Pd^0–NO or N_2O–Mo occurs at 1800 cm^{-1}, and Pd^+–NO species are at 1700 cm^{-1}. The band at 1577 cm^{-1} is attributed to NO_2 formation. These results agree with the explanation of Valden *et al.* (5) for their Pd/Al_2O_3 catalysts, but here the bands are very clear. A band near 2250 cm^{-1} has been attributed to the formation of an Al^{3+}–CO complex (5). The adsorbed NO_2 species are formed when the NO reacts with oxygen bonded to the Pd, which is created by the dissociation of NO. Since the palladium catalyst was prereduced with hydrogen, it favors the formation of strongly bound, bridged Pd_x–NO complexes, as indicated by the small peak around 1800 cm^{-1}, even at 623 K. All these peaks remain after purging with Ar at the same temperature.

Figure 13 compares the results after exposure of the $Pd8Mo/Al_2O_3$ catalyst to NO and to NO + CO at 573 K. First, the band near 2230 cm^{-1}, which corresponds to a isocyanate complex (16), is much larger after the NO + CO reaction. This band did not disappear after purging with Ar and is very stable. It is not attributed to the Al^{+3}–CO formation observed above on the Pd/Al_2O_3 catalyst, because adsorption of CO and NO separately on Pd8Mo indicate this band occurs only for NO adsorption; however, a comparison of the NO and NO + CO absorption bands shows it exhibits a drastic intensity increase during the reaction. The explanation is that in the presence of NO the following reaction occurs to form isocyanate:

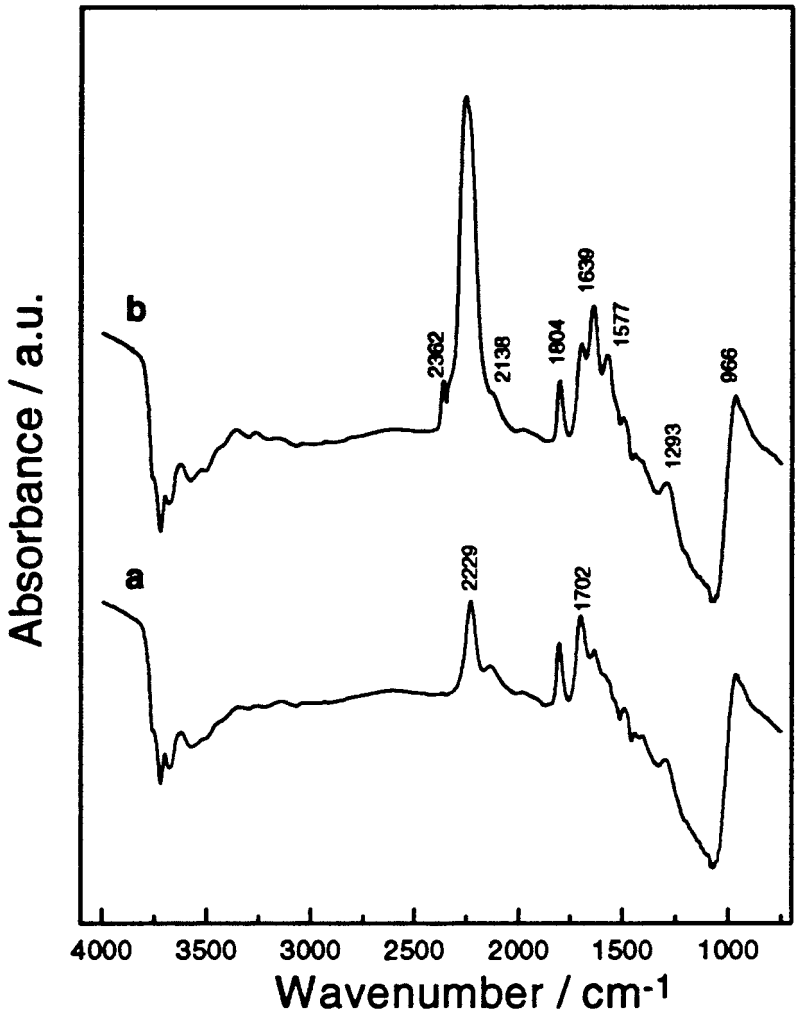

FIG. 13. DRIFT spectra after exposure of Pd8Mo at 573 K to (a) NO and (b) NO + CO.

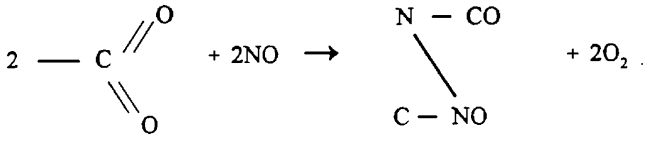

The presence of the N_2O absorption band at 1800 cm^{-1} for N_2O on Mo and the sharp NO absorption bands on Pd at 1701 and 1639 cm^{-1} are remarkable, and they correspond to NO_2 absorption due to the reaction of NO with oxygen associated with the Pd lattice. A CO absorption band on Pd^+ at 2130 cm^{-1} is again present. These bands are very clear and more pronounced compared to those for Pd/Al_2O_3 with the bands between 1491 and 1296 cm^{-1} being attributable to nitrite and nitrate complexes. In addition, bands between 3628 and 3046 cm^{-1} are seen, which are Mo–OH groups associated with molybdate species containing tetrahedral and octahedral configurations, in agreement with the UV-DRS results and in accordance with Knözinger and Ratnasamy (17). These species are very stable, even at higher temperatures.

The conversion of NO during the NO + CO reaction over the Pd/Al_2O_3 and $Pd8Mo/Al_2O_3$ catalysts as a function of the temperature is displayed in Fig. 14, which shows that between 550 and 600 K the conversion over $Pd8Mo/Al_2O_3$ is somewhat higher than that over Pd/Al_2O_3. The better performance with the $Pd8Mo/Al_2O_3$ catalyst is not absolutely new, since Hoost *et al.* (18) have demonstrated that this system is more selective for NO reduction but, contrary to the results here, they observed that this stability is vulnerable. Experiments performed under different reaction conditions using ascending following by descending temperatures have shown that after more than 1 week, the Pd8Mo/Al_2O_3 catalysts were still very stable. The selectivity to N_2 at lower temperatures was high (ca. 87% at 493 K) and remained constant (Table 3). The only other product besides CO_2 and water was N_2O.

However, usually activity and selectivity are the most important parameters to judge catalytic performance. For this system the discussion is a bit difficult, since no parameter is obtained for the determination of the active

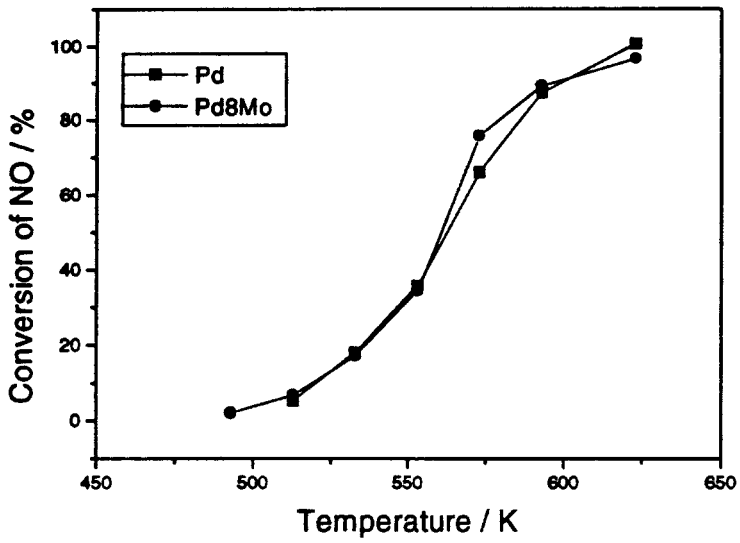

FIG. 14. NO conversion with temperature ($m = 50$ mg, 40 cm^3/min, 0.6% NO + 1.3% CO in He).

sites and thus allow determination of the actual turnover frequencies for comparison with other data in the literature. Reaction rates based on μmoles/s/g_{cat} or μmoles/s/m^2 as reported in the literature are not really applicable in this case (19); however, using the irreversible CO or H_2 uptakes one may calculate TOF values, which represent specific activity and may be quite reasonable for comparison with different systems. The CO adsorption indicates that with increasing Mo content the amount of CO increases, which is attributed to the adsorption on Mo after being submitted to H_2 reduction at 673 K. On the contrary, the H_2 uptake decreases with increasing Mo content, as expected since Pd crystallites may be partially covered by sublayers, as discussed earlier. DRIFTS spectra have shown that CO is adsorbed on metallic Pd while NO adsorbs on Pd^+ or $Mo^{+\delta}$ and reacts to form nitrate or nitrous species and also isocyanate complexes. If we assume that the H_2 uptake is a better indicator of active sites for the NO + CO reaction and that Mo acts as a promoter, then the TOF values in Table 2 are obtained. Figure 15 indicates the specific activity of both systems in terms of the TOF for N_2 formation, based on H adsorption sites, and it shows that the TOF on Pd8Mo/Al_2O_3 is higher than that on Pd/Al_2O_3. Comparing their activities at different temperatures, for example at 573 K, it shows that the specific activity is one-third that of the Mo-containing catalyst. Now, plotting the Arrhenius equation for each system in the range of low conversions, similar activation energies are obtained, as shown in Fig. 16, but different A_0 values exist for each catalyst. The activation energies of 19 to 20 kcal/mole are lower than the values of 29 to 35 kcal/mole found in the literature for this reaction on La_2O_3 and Sr-promoted La_2O_3 catalysts (19).

The selectivity between N_2 and N_2O was monitored for low conversions at 513 K and is displayed in Table 3. Results with different NO molar flow rates show that the selectivity to N_2 was on the order of 46 to 60% over Pd8Mo/Al_2O_3, which is quite good compared to the literature results for NO reduction with CH_4 and CO (20). It is again important to note that this system was very stable.

Different reaction mechanisms have been proposed (21, 22). The effect of a promoter has been discussed by Cordatos and Gorte (23), and they assume that reduction

TABLE 2

Reaction Rates and Selectivities over Pd8Mo/Al_2O_3 at Different Temperatures

T (K)	NO conv. (%)	Rate N_2 (μmol/s/g)	Rate N_2O (μmol/s/g)	N_2 TOF (s^{-1})	Selectivity N_2 (%)	Selectivity N_2O (%)
623	96.7	0.89	1.01	0.72	46	53
593	89.2	0.64	1.11	0.52	36	63
573	75.8	0.58	0.91	0.47	39	61
553	34.4	0.31	0.37	0.25	46	54
533	17.4	0.16	0.18	0.13	46	54
513	6.9	0.075	0.060	0.061	56	44
493	2.1	0.036	0.005	0.030	88	12

TABLE 3

Conversion and Selectivity with Pd8Mo/Al_2O_3 at 513 K

NO conv. (%)	Selectivity to N_2 (%)
22.0	46
13.7	56
11.6	58
10.8	59
10.1	60

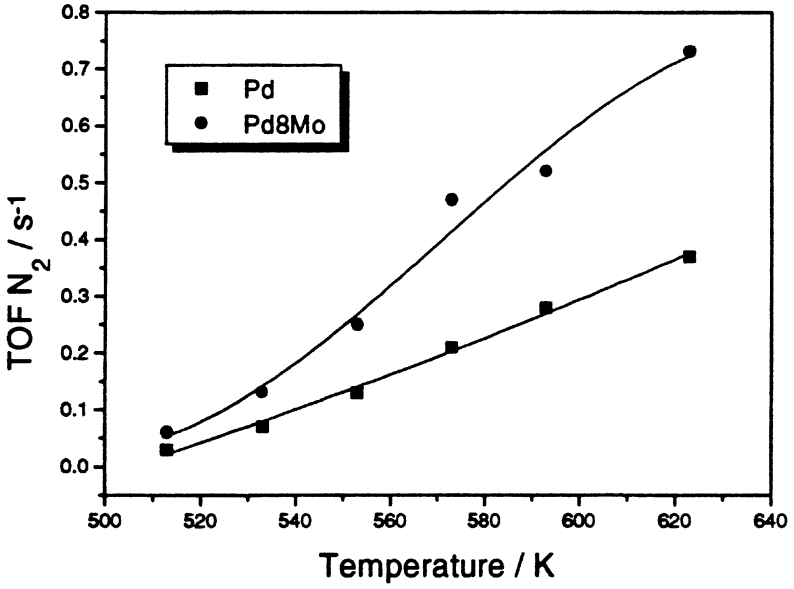

FIG. 15. N_2 TOF for Pd/Al_2O_3 and Pd8Mo catalysts vs temperature ($m = 50$ mg, 40 cm^3/min, 0.6% NO + 1.3% CO in He).

and oxidation of the oxide occurs, in particular with CeO_2 on SiO_2. On the other hand, the DRIFTS spectra indicated NO adsorption, hence an oxidation effect on Mo in reduced form, and clearly CO was adsorbed on reduced Pd particles. These surface phenomena suggest the following sequence of steps to form the reaction product. Initially, CO molecules are chemisorbed on surface Pd^0 atoms, while NO molecules attack the $Mo^{+\delta}$ surface atoms of the Mo sublayer, which are then oxidized to Mo^{+6} and release N_2 as a reaction product. In this sequence, the Pd–CO_{ads} species play an important role, reducing Mo^{+6} to $Mo^{+\delta}$ or Mo^{+4} atoms and releasing CO_2 molecules, and hence regenerating Pd^0 surface atoms via CO adsorption. This mechanism is well represented in Fig. 17 and by the following reaction

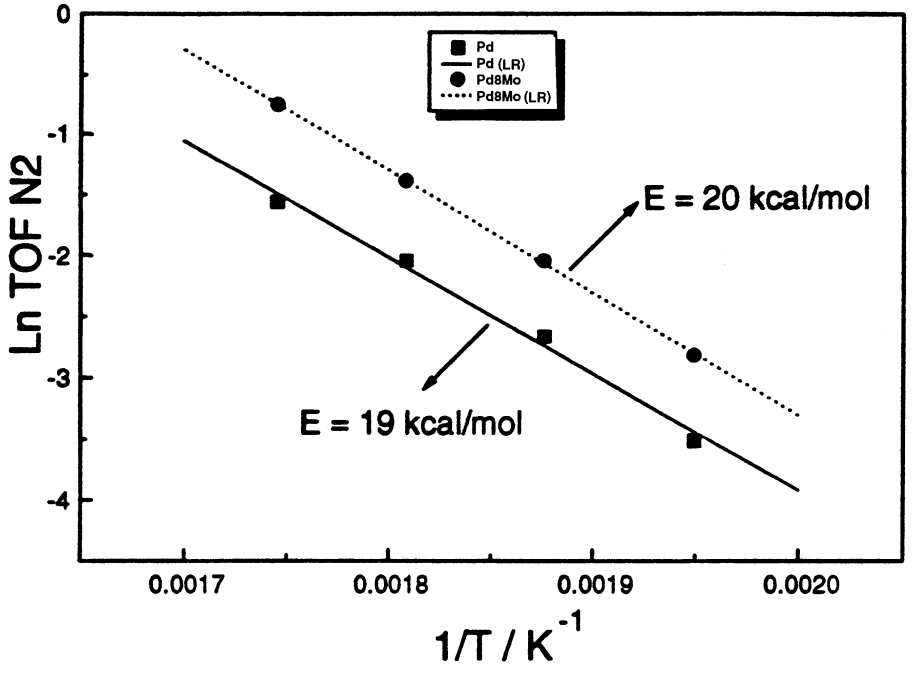

FIG. 16. Arrhenius plots for Pd/Al_2O_3 and Pd8Mo catalysts.

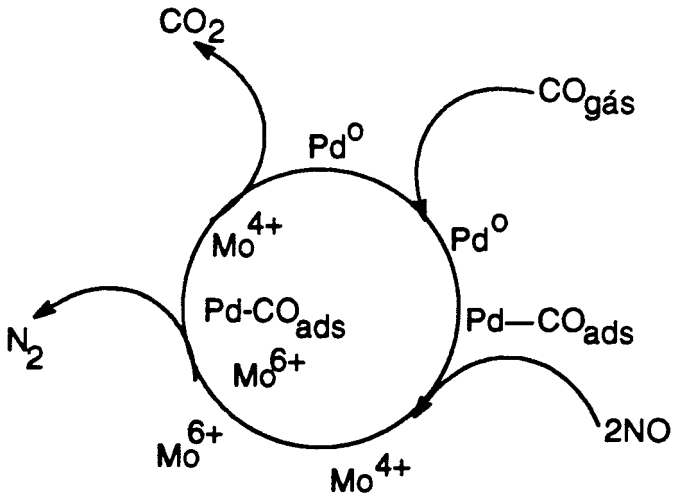

FIG. 17. Mechanism for the CO + NO reaction.

scheme:

$$PdO + H_2 \rightarrow Pd^0 + H_2O \text{ (reduction step)}$$

$$CO + Pd^0 \rightarrow Pd\text{–}CO_{ad}$$

$$2Mo^{+6} + (\delta/2)H_2 \rightarrow 2Mo^{+\delta} + \delta[HO]^-$$

$$2NO + Mo^{+\delta}(Mo^{+4}) \rightarrow N_2 + Mo^{+6}$$

$$Pd^0\text{–}CO_{ad} + Mo^{+6} \rightarrow Mo^{+\delta}(Mo^{+4}) + CO_2 + Pd^0$$

This mechanism assumes that Mo is a promoter which exists as a reducible oxide and reacts with NO. The adsorption of CO molecules on the Mo surface sublayer is indispensable for supplying CO molecules to Pd particles surrounded by Mo. The species around the Pd^0 particles are easily reducible either by H_2 or CO. The larger the number of Mo atoms surrounding the Pd particles, the larger the promotional capability of these Mo species. In addition, the formation of $[OH]^-$ at the surface of Mo promotes formation of Mo–OH species, which also allows the presence of different surface species. On the other hand, the DRIFTS spectra indicate that NO reacts with the Mo surface sublayer and favors the formation of isolated islands of isocyanate species, which can probably explain the stability of this catalyst.

SUMMARY

A Pd8Mo catalyst was prepared with a monolayer of Mo oxide species covering the alumina surface and initially covering the Pd particles dispersed on them. This Mo oxide layer is a result of a polymerization process, identified by UV-DRS measurements. With increasing Mo content, MoO_3 crystals are formed, as shown by XRD and UV-DRS. TPR results indicate the Mo is reduced to Mo^{+4} at lower temperatures in the presence of palladium particles, and this favors the formation of a bimetallic phase creating a different kind of site for this reaction. TPD results indicate that the presence of the Mo monolayer favors the formation of N_2 and reduces N_2O production, and these lineshapes are quite different from those for the Pd/Al_2O_3 catalysts.

DRIFTS spectra indicate NO and CO adsorption on Pd^+, Pd^0, and $Mo^{+\delta}$ sites as well as the formation of isocyanate species on the Pd8Mo catalyst and CO adsorption on Mo monolayers during the reaction at different temperatures. These surface species are very stable. Activity tests showed that the Pd8Mo catalyst has a higher specific activity and is more selective than the monometallic Pd catalyst and that the TOF for N_2 formation based on the H_2 uptake may be a reasonable representation of active sites. A reaction model is proposed that invokes the $Mo^{+\delta}$ species as a promoter surrounding Pd^0 crystallites. CO molecules adsorb on the palladium particles and promote the reduction of Mo^{+6}, while NO induces oxidation of $Mo^{+\delta}$.

ACKNOWLEDGMENTS

Partial support of this study was provided by NSF Grant CTS-9633752. One of us (MS) thanks CNPq for a fellowship to spend six months as a visiting professor in the Chemical Engineering Department at Penn State University. He also acknowledges beneficial discussions with Dr. B. Klingenberg regarding DRIFTS analysis.

REFERENCES

1. Gandhi, H. S., Yao, H. C., and Stepien, H. K., *in* "Catalysis Under Transition Transient Conditions" (A. T. Bell and L. L. Hegedeus, Eds.), ACS Symposium Series, p. 143. American Chemical Society, Washington D.C., 1982.
2. Halasz, I., Brenner, A., Shelef, M., and Ng, K. Y. S., *Appl. Catal. A* **82**, 51 (1992).
3. Halasz, I., Brenner, A., and Shelef, M., *Appl. Catal. B* **2**, 131 (1993).
4. Lange, M., Mergler, Y., and Nieuwenhuys, B., *Catal. Lett.* **35**, 383 (1995).
5. Valden, M., Keiski, L. R., Xiang, N., Pere, J., Aaltonen, J., Pessa, M., Maunula, T., Savimaki, A., Lahti, A., and Harkonen, M., *J. Catal.* **161**, 614 (1996).
6. Szanyi, J., and Goodman, D. W., *J. Phys. Chem.* **98**, 2972 (1994).
7. Baldanza, M. A. S., Amorim, G. S., Pereira, M. A., and Schmal, M., *8th Seminário Brasileiro de Catálise* **1**, 212 (1995).
8. Monteiro, R. S., Tese de Mestrado, NUCAT/PEQ-COPPE/UFRJ, Rio de Janeiro, 1993.
9. Bollinger, M. A., and Vannice, M. A., *Appl. Catal.* **8**, 417 (1996).
10. Fournier, M., Louis, C., Che, M., Chaquin, P., and Masure, D., *J. Catal.* **119**, 400 (1989).
11. Masure, D., Chaquin, P., Louis, C., Che, M., and Fournier, M., *J. Catal.* **119**, 415 (1989).
12. Noronha, F. B., Tese de Mestrado, NUCAT/PEQ-COPPE/UFRJ, Rio de Janeiro, 1989.
13. Rieck, J. S., and Bell, A. T., *J. Catal.* **99**, 262 (1986).

14. Hoang-Van, C., and Zegaoui, O., *Appl. Catal.* **130**, 89 (1995).
15. Stara, I., and Matolin, V., *Surf. Sci.* **313**, 99 (1994).
16. Dompelmann, R., Cant, N. W., and Trimm, D. L., *Appl. Catal. B* **6**, L291 (1995).
17. Knözinger, H., and Ratnasamy, P., *Catal. Rev.-Sci. Eng.* **17**, 31 (1978).
18. Hoost, T. E., Graham, G. W., Shelef, M., Alexeev, O., and Gates, B. C., *Catal. Lett.* **38**, 57 (1996).
19. Huang, S.-J., Walters, A. B., and Vannice, M. A., *J. Catal.* **173**, 229 (1998).
20. Mouaddib, N., Feumi-Jantou, C., Garbowski, E., and Primet, M., *Appl. Catal.* **87**, 129 (1992).
21. Salas-Peregrin, M. A., Primet, M., and Prauliaud, H., *Appl. Catal. B* **8**, 79 (1996).
22. Cho, B. K., *J. Catal.* **148**, 697 (1994).
23. Cordatos, H., and Gorte, R., *J. Catal.* **159**, 112 (1996).